Planar-waveguide integrated spectral comparator

T. W. Mossberg, D. Iazikov, and C. Greiner

LightSmyth Technologies, Inc., 860 West Park, Suite 250, Eugene, Oregon 97401

Received November 17, 2003; revised manuscript received February 10, 2004; accepted February 11, 2004

A cost-effective yet robust and versatile dual-channel spectral comparator is presented. The silica-on-silicon planar-waveguide integrated device includes two holographic Bragg-grating reflectors (HBRs) with complementary spectral transfer functions. Output comprises projections of input signal spectra onto the complementary spectral channels. Spectral comparators may be useful in optical code-division multiplexing, optical packet decoding, spectral target recognition, and the identification of molecular spectra. HBRs may be considered to be mode-specific photonic crystals. © 2004 Optical Society of America

OCIS codes: 050.7330, 130.3120, 230.7390, 230.7400.

Recently, a planar-waveguide-based spectral filtering device, which we refer to as a holographic Bragg reflector (HBR), was proposed.[1] HBRs are distributed reflective structures that may be simplistically thought of as two-dimensional analogs of fiber Bragg gratings[2,3] or channel waveguide gratings.[4,5] Alternatively, HBR structures can be viewed as powerful mode-specific photonic crystals.[6] As they are optical-mode specific, HBR structures can be made physically large or small to accommodate required spectral resolution and available reflective scattering strengths. In this way, HBRs differ from photonic crystals,[7–10] as the latter must utilize highly reflective and typically lossy interfaces so that they can interact with broad ranges of optical modes. The two-dimensional planar-waveguide environment is uniquely different from that found in one-dimensional fiber and channel waveguide environments in that diffractive structures can be implemented to both spectrally filter and spatially route optical signals. Moreover, HBR devices may be fabricated by photolithography or stamping and are therefore consistent with detailed contour-by-contour amplitude and phase apodization, which provides powerful control of spectral transfer functions. HBRs optimally employ 0.25-μm and finer lithographic resolution and utilize the refinements in planar-waveguide materials, homogeneity, and yield achieved over the past decade. HBR fabrication by nanoimprinting offers a path to low-cost production.

Multiple HBRs can be written on a common piece of slab waveguide by superposition, interleaving, or stacking. Each HBR maps a portion of a common input to a separate output with a distinct spectral-transfer function. A dual-HBR structure is shown schematically in Fig. 1. Figure 1(a) is a top view of the slab-waveguide HBR structure. The rectangular outline represents the silica-on-silicon device die. On the left, SMF-28 fibers are butt-coupled at the square-cut die edge to channel waveguides. The central channel waveguide transports signals from the edge of the die to the slab waveguide region where they diffract in the plane to interact with the two HBR structures. Each HBR diffracts back those signal frequencies within its reflective profile, focusing them into an output channel waveguide (top or bottom) that transports the signal to the edge of the die for entry into the butt-coupled fibers. Channel waveguides are 12.7 μm wide at the boundary of the two-dimensional slab-waveguide region and taper adiabatically to 6 μm wide at the die edge. On the die edge, the channel waveguides are separated by 250 μm, but they approach one another until reaching a final 60-μm separation at the interface to the slab-waveguide region. Figure 1(b) shows a cross section of the HBR slab-waveguide region with the diffractive contours etched into the top of the waveguide core region (white region between cladding layers) and filled with cladding material. The separation between adjacent diffractive contours is $\approx$0.5 μm but varies slightly to accommodate the full reflective bandwidth of the HBR. The HBRs operate in first reflective order so resonant portions have contour spacings determined by $\lambda/2n_{\mathrm{eff}}$, where λ is the reflected wavelength and n_{eff} is the effective slab-waveguide refractive index. The silica core (cladding) layers are 2 μm (15 μm) thick and the diffractive contours are etched $\approx$450 nm deep. The core–cladding index contrast is $\approx$0.8 percent. Figure 1(c) shows a photograph of a fabricated spectral comparator. For demonstration purposes the specimen in the photograph has no upper cladding. The entire HBR diffractive structure is approximately 20 mm long. The generally vertical bands of Fig. 1(c) correspond to individual spectral peaks within the spectral transfer functions of the two channels as described below. Each HBR spans the full device length so that subsections of the two HBRs are interleaved. Interleaving of HBRs rather than direct overwrite or sequential stacking offers advantages when one wishes to avoid complications of intersecting lithographic structures and–or achieve a spectral resolution set by the full device length. HBR devices tested in this work have computer-generated contours that were laser-written to a reticle and fabricated with a deep-ultraviolet, quarter-micrometer-resolution, 4-to-1-reduction, photolithographic stepper. Both HBR structures were written onto a single reticle.

Amplitude apodization of the HBR is introduced by using the partial fill method,[11,12] in which trenches are written only on portions of diffractive contour lines, i.e., the curved contours shown in Fig. 1(a) are actually created in

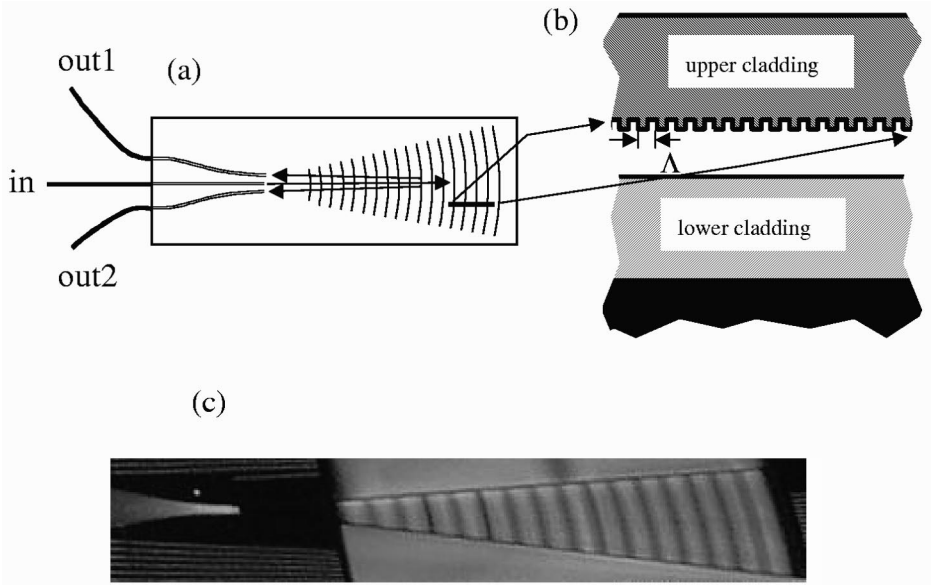

Fig. 1. (a) Schematic top view of a two-channel holographic Bragg reflector with channel waveguide inputs and etched diffractive contours. (b) Cross section showing slab-waveguide region and etched diffractive contours. Some contours of the actual devices are written as dashed lines for diffractive amplitude control. For the devices considered here the grating period $\Lambda \approx 0.5\ \mu$m. (c) Photograph of fabricated two-channel spectral comparator. For purposes of demonstration the device photographed has no upper cladding.

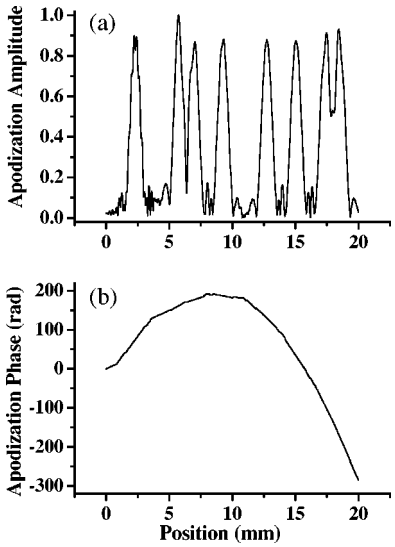

Fig. 2. Phase and amplitude apodization profiles employed for one of the spectral comparator's two channels. Amplitude (phase) apodization is implemented through partial contour writing (spatial displacement of contours).

the form of dashed lines. The spacing and pattern of the dashed (etched) contour portions are controlled so that the focusing property of the contour is not compromised. Amplitude apodization by partial contour scribing is made possible by the fact that output signals consist of an integral over the full contour and therefore scale in proportion to the fraction of the contour etched. Partial-fill apodization is consistent with constant-depth etching, which is important from the perspective of simple lithographic scribing. A more extensive description and analysis of partial-fill amplitude apodization is given in Ref. 11. Phase apodization is effected by introducing relative spatial displacements of individual contours. In Fig. 2(a) [2(b)] we plot the amplitude [phase] apodization function used in fabricating one of the HBRs that constitute the dual-channel spectral comparator. The horizontal scale in Fig. 2 corresponds to the depth into the HBR device, with zero corresponding to the location of the first contour on the channel waveguide side (see Fig. 1). Apodization amplitudes shown in Fig. 2(a) represent the fraction of each HBR diffractive contour that is written (as in a dashed line). The phases of Fig. 2(b) are relative to a fixed-period reference grating. Note that the overall paraboliclike phase evolution corresponds to a stepwise chirp in diffractive element spacing. Thus successive peaks in Fig. 2(a) correspond to successive spectral peaks. Both amplitude and phase apodization functions are designed to minimize coherent beating between the different peaks in the spectral transfer function. Note in Fig. 2(a) that the apodization amplitude for the HBR channel shown exhibits valleys. The apodization peaks for the complementary channel fall in those valleys. Spatial overlap of the two HBRs occurs in regions of low apodization amplitude for both. In these regions, contours are mostly unwritten so that physical contour overlap is negligible.

In Figs. 3(a) and (b) we present the measured spectral transfer functions of the two HBR channels. Insertion loss shown is relative. Minimum absolute insertion loss of 8 dB includes that due to fiber-to-channel-waveguide coupling ($\approx$1 dB). Transmission measurements show that remaining insertion loss arises primarily from low HBR reflectivity rather than scattering loss or absorption. Changes in internal waveguide and diffractive contour design—for example, slightly increasing the core–cladding refractive-index contrast or increasing the aspect ratio of the diffractive contour trenches—should provide substantially higher reflectivity. Aspect ratios of four have been demonstrated in more advanced designs. In Fig. 3(c) we present the summed spectral throughput of the two HBR channels. As is apparent from the figure,

the transfer functions of the two HBR channels are complementary. Output signals from the dual-HBR spectral comparator represent projections of input signal spectra onto the two complementary spectral transfer functions shown in Figs. 3(a) and 3(b).

In Fig. 4 we provide a detailed simulation of one of the HBR spectral transfer functions. Figure 4(a) shows the

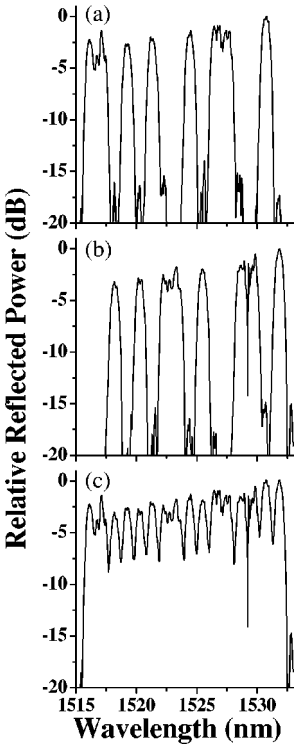

Fig. 3. (a), (b) Measured spectral transfer functions of the device's two channels. (c) Summed spectra of both channels.

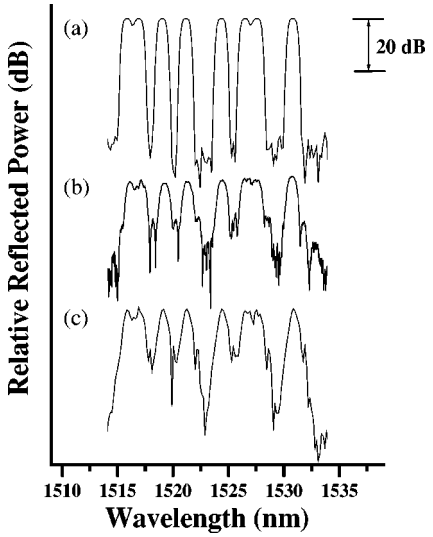

Fig. 4. Comparison of measured and designed spectral transfer functions. (a) Channel spectrum as designed without accounting for amplitude-apodization-induced effective waveguide refractive-index variations. (b) Measured channel spectrum. (c) Channel spectrum as simulated from fabricated device design and accounting for amplitude-apodization-induced effective waveguide refractive-index variations.

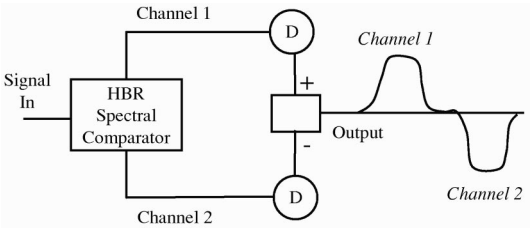

Fig. 5. Schematic depiction of a spectral comparator based on the device described here that provides analog comparison of input signal spectra to reference spectra encoded on device channels 1 and 2. The polarity of the output signal indicates which of the comparator spectral channels most closely matches the unknown input signal spectra.

device transfer function expected on the basis of the apodization function of Fig. 2 implemented in a slab waveguide of constant effective refractive index. The simulation is performed with an exact numerical model of the HBR structure as taped out for fabrication by using a Fresnel diffraction approach. Figure 4(b) depicts the measured transfer function. Some deviations from expectation are found. Analysis reveals that the deviations arise from an effect that was not accounted for in the implemented design algorithm. The amplitude apodization approach we employed has a second-order effect, but one that is highly predictable and therefore amenable to inclusion in the design algorithm. This second-order effect consists of a small change in effective waveguide refractive index concomitant with changes in the apodized diffractive amplitude.[13] Measurements of ancillary devices provide a calibration of the magnitude of the effect. By incorporating effective index changes introduced by amplitude apodization into the simulation model—with no adjustable parameters—one predicts the spectral transfer function of Fig. 4(c). Agreement with the measured spectral transfer function is quite good, implying that designs accounting for apodization-induced refractive-index variations will be accurately realized.

Measurements of the HBR spectral transfer functions were performed with polarized light. No significant polarization-dependent loss was observed; however, polarization-dependent spectral shifts of ≈ 0.6 nm (corresponding to a fractional birefringence of $\approx 4 \times 10^{-4}$) were. Auxiliary measurements indicate that these shifts arise from residual slab waveguide birefringence rather than intrinsic HBR function.[12] Changes in annealing procedures or use of channel-waveguide-sampled HBRs may provide a means of eliminating residual slab-waveguide birefringence effects.[12] Note that birefringence in channel waveguides has been successfully reduced by others.[4]

In Fig. 5 we depict schematically how a two-channel HBR might be implemented in a simple circuit to form a spectral comparator (this circuit is for pedagogical purposes only and was not implemented in our current work). If the input signal has a spectrum that matches that of channel 1, the output signal goes high. Conversely, if the input signal has a spectrum that matches channel 2, the output signal goes low. If the input signal spectrum is white, the output signal is zero. Comparator function such as this may be useful in multiple areas including spectral signature recognition and optical code division

multiple access.[14] We note that other spectral encoding and decoding approaches have been introduced.[15–17] These approaches utilize variations of arrayed waveguide grating technology. HBR-based comparators differ significantly from those based on arrayed waveguide gratings in that many spectral transfer functions can be recorded on a single die so that an input signal may be simultaneously compared to multiple spectra. HBR-based comparators also tend to be smaller since spectral resolution is set by the full device size, while arrayed waveguide gating resolution is set by optical path differences that are a small fraction of the overall device size. We expect that 32–64 different spectral transfer functions may be recorded on a single HBR-based comparator die of 5×20 mm. In terms of fabrication, HBR devices optimally require higher lithographic resolution (0.25 μm versus several micrometers), but quarter-micrometer, deep-ultraviolet lithography is now standard. Unlike waveguide-based devices, holographic structures are essentially immune from point fabrication defects, potentially providing higher yield. Since HBRs are smaller for the same spectral resolution, waveguide refractive index and related wafer factors do not have to be uniform over as large an area. We also note that HBR comparator channels need not be complementary.

It is interesting to determine the degree of spectral complexity that the HBR comparator channels can be programmed to recognize. This matter is governed by two primary considerations. First is the total bandwidth over which the HBR can be configured to provide reflectivity at the level required for a particular application. We call this bandwidth Δ_T. Second is the spectral resolution width of the HBR, which we denote Δ_R. It can be shown that for a first-order HBR structure with reflectivity level of 80–90 percent[6,13]

$$\Delta_T \approx \frac{cL_{\text{eff}}\Delta n^2 q^2}{4\Lambda^2 n^3}, \tag{1}$$

where c is the vacuum light speed, L_{eff} is the effective fully written length of the HBR (total HBR length multiplied by the average amplitude apodization value, where unity amplitude is a fully written contour), Δn is the refractive-index contrast at the face of HBR diffractive elements (grating contours), Λ is the average grating spacing, n is the effective waveguide refractive index, and q is a form factor determined by the geometry of the diffractive structures and is equal to the ratio of the modal field backscattered by the HBR diffractive elements to that which would be backscattered by planar interfaces spanning the entire waveguide mode. For the HBRs fabricated here, $q \approx 0.06$. It can also be shown that the spectral resolution (minimum spectral feature width) of a spatially coherent HBR of total length L is

$$\Delta_R = \frac{c}{2nL}. \tag{2}$$

It has been demonstrated that HBR devices of up to centimeter scale can be fabricated with full spatial coherence. In general, the quantity L in Eq. (2) should be identified with the spatial coherence length of the HBR structure, which may be equal to the physical HBR length or shorter. The ratio $S \equiv \Delta_T/\Delta_R$ gives a measure of how much spectral complexity can be programmed into the reflection profile of a single HBR. For example, to represent a molecular spectrum having 100 distinct lines requires an S value of $\approx$100. Large values of S imply that the reflection spectrum of an individual HBR can assume a very complex yet precisely controllable profile. We can write

$$S \equiv \frac{\Delta_T}{\Delta_R} \approx \frac{LL_{\text{eff}}\Delta n^2 q^2}{2\Lambda^2 n^2}. \tag{3}$$

For $L_{\text{eff}} = 0.007$ m, $L = 0.02$ m, $\Delta n = 0.01$, $\Lambda = 0.53$ μm, $n = 1.45$, and $q = 0.06$ (estimated for our diffractive elements), we find $S \approx 43$. Converting frequency intervals Δ_T and Δ_R into wavelength intervals $\Delta\lambda_T$ and $\Delta\lambda_R$ according to $\Delta\lambda_x = 4n^2\Lambda^2\Delta_x/c$, we have $\Delta\lambda_T \approx 1.7$ nm and $\Delta\lambda_R \approx 0.04$ nm. In our fabricated device, we designed for a larger reflection bandwidth and broader spectral channel (feature) widths; therefore it does not exhibit the high reflectivity or higher spectral feature count that would have been possible if it had been designed to realize calculated $\Delta\lambda_T$ and $\Delta\lambda_R$ values. The parameter S defined by relation (3) can be seen to depend sensitively on multiple controllable parameters, including Δn and q. Increase of Δn by 3 and q by 2 (through deeper etch, for example) drives the S parameter to the vicinity of 2000, which means that optimized devices should support very complex spectral profiles, including high-resolution molecular spectra.

In summary, we have demonstrated a dual-channel integrated device whose two outputs represent the projection of input signals onto complementary spectral references. An estimate of the spectral complexity that can be encoded into HBR devices has been given in terms of device parameters, indicating that quite complex spectral functions (including, for example, molecular spectra) can be encoded. Depending on parameters, additional spectral channels can be added to the device to provide for real-time comparison of input spectra against a multitude of stored reference spectra.

Corresponding author T. W. Mossberg's e-mail address is twmoss@lightsmyth.com.

REFERENCES

1. T. W. Mossberg, "Planar holographic optical processing devices," Opt. Lett. **26**, 414–416 (2001).
2. T. Erdogan, "Fiber grating spectra," J. Lightwave Technol. **15**, 1277–1294 (1997).
3. A. Othonos, "Fiber Bragg gratings," Rev. Sci. Instrum. **68**, 4309–4341 (1997).
4. R. Adar, C. H. Henry, R. C. Kistler, and R. F. Kazarinov, "Polarization independent narrowband Bragg reflection gratings made with silica-on-silicon waveguides," Appl. Phys. Lett. **60**, 1779–1781 (1992).
5. D. Wiesmann, R. Germann, G. L. Bona, C. David, D. Erni, and H. Jackel, "Add–drop filter based on apodized surface-corrugated gratings," J. Opt. Soc. Am. B **20**, 417–223 (2003).
6. A. Yariv and P. Yeh, *Optical Waves in Crystals* (Wiley, New York, 1984).
7. D. Labilloy, H. Benisty, C. Weisbuch, T. F. Krauss, D. Cassagne, C. Jouanin, R. Houdre, U. Oesterle, and V. Bardinal,

"Diffraction efficiency and guided light control by two-dimensional photonic-bandgap lattices," IEEE J. Quantum Electron. **35**, 1045–1052 (1999).
8. A. Giorgio, A. G. Perri, and M. N. Armenise, "Modeling of fully etched waveguiding photonic bandgap structures," IEEE J. Quantum Electron. **38**, 630–639 (2002).
9. D. M. Pustai, A. Sharkawy, S. Shi, G. Jin, J. Murakowski, and D. W. Prather, "Characterization and analysis of photonic crystal coupled waveguides," J. Microlith. Microfab. Microsyst. **2**, 292–298 (2003).
10. S. Rowson, A. Chelnokov, and J. M. Lourtioz, "Two-dimensional photonic crystals in macroporous silicon: from midinfrared (10 μm) to telecommunication wavelengths (1.3–1.5 μm)," J. Lightwave Technol. **17**, 1989–1995 (1999).
11. D. Iazikov, C. Greiner, and T. W. Mossberg, "Effective gray-scale in lithographically-scribed planar holographic Bragg reflectors," Appl. Opt. **43**, 1149–1155 (2004).
12. C. Greiner, D. Iazikov, and T. W. Mossberg, "Lithographically-fabricated planar holographic Bragg reflectors," J. Lightwave Technol. **22**, 136–145 (2004).
13. D. Iazikov, C. Greiner, and T. W. Mossberg, "Apodizable integrated filters for coarse WDM and FTTH-type applications," J. Lightwave Technol. (to be published).
14. T. W. Mossberg and M. G. Raymer, "Optical code division multiplexing," Opt. Photon. News **12**, 50–55 (2001).
15. K. Takiguchi, T. Shibata, and M. Itoh, "Encoder/decoder on planar lightwave circuit for time-spreading/wavelength-hopping optical CDMA," Electron. Lett. **38**, 469–470 (2002).
16. C. H. Lee, S. Zhong, X. Lin, J. F. Young, and Y. J. Chen, "Planar lightwave circuit design for programmable complementary spectral keying encoder and decoder," Electron. Lett. **35**, 1813–1815 (1999).
17. H. Tsuda, H. Takenouchi, T. Ishii, K. Okamoto, T. Goh, K. Sato, A. Hirano, T. Kurokawa, and C. Amano, "Spectral encoding and decoding of 10 Gbit/s femtosecond pulses using high resolution arrayed-waveguide grating," Electron. Lett. **35**, 1186–1188 (1999).